A Methodology for the Estimation and Modelling of the Obstruction Factor in the Expression for Mesopore Diffusion in Reversed-Phase Liquid Chromatography Particles

Song, Huiying; Desmet, Gert; Cabooter, Deirdre

Published in:
Journal of Chromatography A

DOI:
10.1016/j.chroma.2020.461285

Publication date:
2020

License:
CC BY-NC-ND

Document Version:
Accepted author manuscript

A Methodology for the Estimation and Modelling of the Obstruction Factor in the Expression for Mesopore Diffusion in Reversed-Phase Liquid Chromatography Particles

Huiying Song[(1)], Gert Desmet[(2)], Deirdre Cabooter[(1,*)]

[(1)]University of Leuven (KU Leuven), Department for Pharmaceutical and Pharmacological Sciences, Pharmaceutical Analysis, Herestraat 49, Leuven, Belgium

[(2)]Vrije Universiteit Brussel, Department of Chemical Engineering, Pleinlaan 2, 1050 Brussel, Belgium

(*) corresponding author:

tel.: (+) 32 (0)16.32.34.42, fax: (+) 32 (0)16.32.34.48, e-mail: deirdre.cabooter@kuleuven.be

Abstract

An experimental methodology for the determination of the obstruction factor in the expression for mesopore diffusion in Zorbax Eclipse Plus C_{18} reversed-phase particles is proposed. The method uses peak parking experiments conducted on particles that were previously stripped of their stationary phase by flushing the column with trifluoroacetic acid at a temperature of 60°C. Further using pure organic solvents as the mobile phase, any potential retention or surface diffusion effect is omitted. To avoid interference between the parked peaks and baseline disturbances typically occurring when switching on and off the flow, peak parking experiments were carried out in a set-up wherein two identical columns were used in parallel. This set-up allowed to maintain the flow through the detector at all times, by redirecting the flow from one column to the other during the peak parking experiments. Several tracer molecules (ionic and deuterated tracers) were compared and it was found that the use of deuterated molecules provides the best possible coverage of the accessible space of the mesopore volume. Interpreting the peak parking responses obtained with these tracers with a model based on the effective medium theory (EMT) subsequently provided an estimate of the value of the mesopore diffusion obstruction factor γ_{mp}. Taking the well-established pore hindrance factor $F(\lambda)$ correction into account, the obtained experimental γ_{mp}-values are more in agreement with the tortuous and constricted diffusion paths one can expect in the void space within a structure resembling a monolithic skeleton with tetrahedral connectivity rather than in the void space formed by a packing of nanospheres. This is also more in line with the measured internal porosity values lying around ε_{pz}=0.5, whereas a packing of nanospheres would rather correspond to an ε_{pz} of 0.4. As such, the presented protocol provides a means to infer the internal mesopore structure of reversed-phase particles.

Keywords: mesopore diffusion; mass transfer; effective medium theory; peak parking; column kinetics; intra-particle diffusion

1. Introduction

Ongoing efforts in liquid chromatography (LC) column technology are focused on the development of faster and more efficient separations. To guide this research, an in-depth comprehension of the mass transfer kinetics in LC is primordial. This requires a thorough understanding of the individual contributions to band broadening. Among many successful semi-empirical models that fit band broadening data in packed beds well, the following equation was recently proposed [1]:

$$h = h_{inhom} + \frac{2}{\nu_i}\frac{D_{eff}}{D_m}(1+k") + \frac{2}{\alpha}\frac{k"^2}{(1+k")^2}\frac{\varepsilon_e}{1-\varepsilon_e}\frac{\nu_i}{Sh_m} + \frac{2}{\alpha}\frac{k"}{(1+k")^2}\frac{\nu_i}{Sh_{part}\frac{D_{pz}}{D_m}} \quad (1)$$

Wherein the first term relates to band broadening originating from flow heterogeneities in the packed bed, or eddy dispersion, the second term is the effective longitudinal diffusion term and the third and fourth term, the resistance to mass transfer in the mobile and stationary zone, respectively. In Eq. (1), h is the reduced plate height, ν_i the reduced interstitial velocity, D_{eff}, D_{pz} and D_m are the effective, mesoporous zone and bulk molecular diffusion coefficients, respectively, k" is the zone retention factor, ε_e the external porosity, α a geometrical constant (equal to 6 for spherical particles), and Sh_m and Sh_{part} the Sherwood numbers (dimensionless mass transfer coefficients) relating to the mobile and the intra-particle zone, respectively.

In order to reach their interaction sites within the particles, which is indispensable for retention, analytes move through the mesopores via intra-particle or mesoporous zone diffusion (depicted by D_{pz} in Eq. (1)). Miyabe and Guiochon demonstrated that intra-particle diffusion, and in particular surface diffusion, has an important impact on band broadening in LC columns, and makes up approximately 30% of the overall band broadening of 5 µm particle columns at high flow rates [2]. A better understanding of intra-particle mass transfer kinetics is hence in order for a better comprehension of band broadening. Mesoporous zone or intra-particle diffusion is typically subdivided in a contribution originating from stationary phase diffusion ($\gamma_s D_s$) and pore diffusion ($\gamma_{mp} D_m$) [3], wherein both are usually considered to occur in parallel. This parallel-zone model assumes that diffusion inside the particle pores is comparable to diffusion in a network of straight, parallel, cylindrical tubes, where diffusion only takes place inside the pores and not through the solid pore walls [4]. In the parallel-zone model, D_{pz} is calculated as a residence-time weighted addition of both contributions:

$$D_{pz} = \frac{\varepsilon_{pz}\cdot\gamma_{mp}D_m + (1-\varepsilon_{pz})K_{A,pz}\cdot\gamma_s D_s}{\varepsilon_{pz} + (1-\varepsilon_{pz})K_{A,pz}} \quad (2)$$

In Eq. (2), ε_{pz} is the intra-particle or mesoporous zone porosity and $K_{A,pz}$ the solid phase-based equilibrium constant:

$$K_{A,pz} = \left(\frac{1}{1-\varepsilon_{pz}}\right)\left(\frac{k^{''}\varepsilon_e}{1-\varepsilon_e} - \varepsilon_{pz}\right) \quad (3)$$

Stationary phase diffusion ($\gamma_s D_s$) describes the movement of the analyte molecules along the surface of the stationary phase, while in an adsorbed state. Since stationary phase diffusion occurs in the adsorbed state, it depends on the retention of the analyte, and hence on the physicochemical properties of the analyte, the mobile phase and the stationary phase. The importance of stationary phase diffusion on intra-particle diffusion and band broadening in general was already pointed out by Giddings in 1965 [5] and its mechanism is now fully understood [6–8].

Pore diffusion, on the other hand, does not involve any interaction between the analytes and the inner walls of the mesopores, and is driven by the concentration gradient of the analytes as they diffuse through the stagnant mobile phase in the mesopores [2]. In Eq. (2), γ_{mp} is generally calculated in terms of the pore hindrance factor F(λ), describing the drag a diffusing molecule experiences due to the confinement within the pore walls as well as steric exclusion, and the obstruction factor resulting from the tortuosity and constriction of the pore space $\frac{1}{\tau^2}$ [9]:

$$\gamma_{mp} = \frac{F(\lambda)}{\tau^2} \quad (4)$$

Where τ represents the pore tortuosity and λ the ratio of the molecular diameter of the analyte to the pore diameter. Note that F(λ) becomes 1 (no hindrance) when λ is 0 (hence for small analytes in large pores). Different expressions are available in the literature to calculate F(λ) [4,10–14]. Typical expressions, such as the Brenner and Gaydos, the Haberman and the Renkin expression, are obtained by calculating the drag force a spherical particle undergoes when moving near a solid wall [12,13]. These expressions assume the analyte behaves as a hard sphere moving near the wall of a cylindrical tube, and are therefore crude approximations of the actual situation (with a typical uncertainty of 10-20%). The pore obstruction factor, corresponding to the inverse of the square of the pore tortuosity ($1/\tau^2$) as represented in Eq. (4), is usually estimated by assuming the meso-porous zone can be represented as a packing of non-porous nanospheres.

Several expressions based on the effective medium theory (EMT) exist that can be used to estimate $1/\tau^2$ (for an overview of such expressions, the reader is kindly referred to [9]). One of the main difficulties to evaluate such expressions in practice is the inherent difficulty to assess the sole contribution of pore diffusion, without any influence of other mass transfer contributions (in this case specifically, stationary phase diffusion) [15].

We recently developed a protocol wherein the C_{18} stationary phase of reversed-phase columns was stripped away in order to study the effects of band broadening under RPLC and HILIC conditions under identical packing conditions [3,16]. In the current contribution, we used the same columns without C_{18} stationary phase to measure the pure effects of pore diffusion, devoid of any influence of stationary phase diffusion. For this purpose, peak parking experiments were conducted using mobile phases consisting of a single solvent (acetonitrile, methanol or an aqueous buffer) to measure the effective diffusion coefficient of small molecules (deuterated acetonitrile, deuterated methanol or $NaNO_3$), able to penetrate the mesoporous volume as well as possible, with a minimal pore hindrance. It was assumed that, using a single solvent as mobile phase and columns that were stripped of their stationary phase, these small molecules would show no retentivity and hence no stationary phase diffusion. This allowed to directly deduce the values of pore diffusion from the experimentally measured effective diffusion coefficients, since $K_{A,pz}$ in Eq. (2) is effectively zero under the present conditions such that Eq. (2) directly yields $D_{pz}= \gamma_{mp}D_m$. It was subsequently investigated whether the values of γ_{mp} could be modelled to an expression based on the effective medium theory.

Denoyel et al. previously used a similar approach to measure and model pore diffusion, and more specifically deduce values of the pore tortuosity, for bare silica particles with particle sizes of 10-12 µm, using toluene and polystyrene standards as probes, and tetrahydrofuran as the mobile phase to avoid any adsorption of the probes onto the stationary phase [17,18]. They demonstrated that the pore tortuosity can be modeled via the Weissberg equation:

$$\tau^2 = 1 - p \cdot ln\varepsilon_{pz} \quad (5)$$

wherein p is a value specific to the pore topology. The authors reported p-values ranging between p= 0.5 (for a mesopore structure resembling a distribution of hard spheres) and p= 2.4 (for columns with a pore structure that is more complex than a simple aggregation of spheres).

With our study, we aim to update and extend this work to modern reversed-phase columns by removing their stationary phase and performing diffusion measurements in the thus obtained stripped particles. In contrast with previous work, this allows to eliminate any influence of stationary phase diffusion [15], while it also allows to perform these measurements in columns that have the same macroporous structure as the original reversed-phase packing [19]. In this way, an experimental protocol for the measurement and subsequent modelling of mesopore diffusion is obtained. In a follow-up study, the thus obtained expression will, together with a new expression for stationary phase diffusion, serve as the basis for the determination of intra-particle diffusivity in reversed-phase columns. It should be stressed that, when adopting this approach, it is assumed that the tortuosity of the alkyl-coated mesopore space is the same as that of the mesopore space in the stripped particles (the volumetric reduction caused by the presence of the alkyl chains is accounted for by the ε_{pz}-factor appearing in Eq. (2) but the value of γ_{mp} is assumed to be the same in both stripped and non-stripped conditions). Note that this is currently assumed in all models for intra-particle diffusion (cfr. the simple addition of the mesopore and stationary-phase diffusion in all models in literature, see also Eq. (2)). This independence corresponds to saying that the tortuous path of the molecules is not altered by the presence of the C_{18} layer. This is an assumption that is justified if the stationary phase is conformal with the structure of the silica mesopore walls, which seems, given the monolayer character of the layer, a good assumption. This assumption seems to be confirmed by the work of Schure et al. based on Monte Carlo simulations wherein it was demonstrated that octadecyl chains predominantly adopt an extended but not all-trans conformation with an average end-to-end distance or bonded phase thickness of around 15 Å [20,21]. This was observed for different water-acetonitrile mixtures, although it was observed that the end-to-end distance slightly increases as the concentration of organic modifier increases. Sander et al. reported a similar average thickness of 17 Å for a monomeric C_{18} bonded phase in methanol using small angle neutron scattering [22].

2. Theory

The intra-particle diffusion coefficient can relatively easily be deduced from the effective or longitudinal diffusion coefficient that can be determined via peak parking experiments. Protocols to execute such peak parking experiments and consecutively deduce the effective diffusion coefficient (D_{eff}) have been amply described in literature [15,23–27]. Knowledge of D_{eff} subsequently allows to extract the intra-particle diffusion coefficient (D_{pz}) by modelling the experimentally measured values of D_{eff} to an expression based on the effective medium

theory (EMT), which postulates that diffusion in a binary medium consisting of two phases with different transport rates (in this case, the interstitial zone outside the particles and the intra-particle zone) occurs at a rate that is in between a purely parallel-connection rate (where the diffusion inside and outside the particles occur simultaneously and independent of each other) and a purely serial-connection rate (where diffusion inside and outside the particles occur sequentially and the overall diffusion rate is dominated by the slowest zone) [28]. Examples of EMT-based expressions are the first-order accurate Maxwell equation [29]:

$$\frac{D_{eff}}{D_m} = \frac{1}{\varepsilon_e(1+k'')} \frac{1+2\beta_1(1-\varepsilon_e)}{1-\beta_1(1-\varepsilon_e)} \quad (6)$$

and the second-order accurate Torquato equation:

$$\frac{D_{eff}}{D_m} = \frac{1}{\varepsilon_e(1+k'')} \frac{1+2\beta_1(1-\varepsilon_e)-2\varepsilon_e\zeta_2\beta_1^2}{1-\beta_1(1-\varepsilon_e)-2\varepsilon_e\zeta_2\beta_1^2} \quad (7)$$

In Eq. (7), ζ_2 is a geometrical three-point parameter that depends on the particle fraction ($1-\varepsilon_e$) and β_1 is the polarizability constant. Experimentally obtained values of D_{eff} and ε_e, that can for example be obtained via total pore blocking experiments [30,31], allow to extract the value of β_1. Subsequently employing Eq. (8), the value of the relative particle permeability α_{part} can be calculated:

$$\alpha_{part} = \frac{1+2\cdot\beta_1}{1-\beta_1} \quad (8)$$

For fully porous particles, this leads to the value of D_{pz} using the following expression:

$$D_{pz} = \alpha_{part} \cdot \frac{1-\varepsilon_e}{\varepsilon_e k''} \cdot D_m \quad (9)$$

3. Experimental

3.1. Chemicals and columns

$NaNO_3$, deuterated methanol (CD_3OD), deuterated acetonitrile (CD_3CN) and ammonium formate were obtained from Sigma-Aldrich (Steinheim, Germany). Milli-Q water was prepared in the lab using a Milli-Q gradient water purification system from Millipore (Bedford, MA, USA). LC-MS grade acetonitrile (ACN) and methanol (MeOH) were purchased from VWR Belgium (Leuven, Belgium). LC-MS grade formic acid was from Merck (Darmstadt, Germany). Two Zorbax Eclipse Plus C_{18} (4.6 × 50 mm, d_p = 5 µm) fully porous particle columns (stripped column 1 and stripped column 2) were obtained from Agilent Technologies (Diegem, Belgium). Zorbax particles are manufactured via coacervation, meaning that uniform-sized, inorganic

colloidal silica particles are associated by a polymerizable organic material into spherical microparticles. This results in a lightly interconnected three-dimensional network of inorganic material surrounding a plurality of uniform-sized pores [32]. Some specific parameters of these columns are given in Table 1. The C_{18} stationary phase of the RPLC columns was stripped away using the protocol described in [16].

3.2. Apparatus

All peak-parking experiments and D_m measurements were performed on an Agilent 1290 UHPLC system (Agilent Technologies, Waldbronn, Germany) equipped with a quaternary pump, autosampler and diode array detector (DAD) with a flow cell of 1 µL. The extra-column volume of the UHPLC instrument was 12 µL. The UHPLC instrument was coupled to a triple quadrupole mass spectrometer (API 3000, Applied Biosystems, Carlsbad, CA, USA), equipped with an electrospray probe working in positive mode, using a piece of PEEK tubing with an I.D. of 127 µm and a length of 50 mm. Source dependent parameters were optimized in flow injection analysis (FIA) at 0.2 mL/min using the corresponding mobile phase compositions. The source dependent parameters are summarized in Table 2. Chemstation software (Agilent Technologies) was used to control the UHPLC system. Analyst 1.5.2 version (AB Sciex) was used to control the mass spectrometer and for data acquisition. Recorded peaks were analyzed with an in-house written Matlab program that determines the first moment and peak variances using the method of moments [33].

For the peak parking experiments using $NaNO_3$ (10 mg/mL) as the test molecule, the UV detector was used at a wavelength of 254 nm. For the peak parking experiments using CD_3OD and CD_3CN as the test molecules, the triple quadruple mass spectrometer was used as the detector and the corresponding parameters are shown in Table 2. The injection volume was 1µL, the flow rate was 0.2 mL/min.

3.3. Methodology

Peak parking experiments were executed in RPLC columns that were stripped of their stationary phase, using pure CD_3CN as the test molecule in a mobile phase consisting of pure ACN, pure CD_3OD as the test molecule in a mobile phase consisting of pure MeOH, and $NaNO_3$ as the test molecule in a mobile phase consisting of 20 mM ammonium formate (brought to pH 2.7 with formic acid). All measurements were performed four times for each peak parking time, and the

variances in time coordinates (σ^2_t) obtained from the chromatograms were subsequently transformed into variances in spatial coordinates (σ^2_x) as follows:

$$\sigma_x^2 = \sigma_t^2 \left[\frac{L}{t_i(1+k")}\right]^2 \quad (10)$$

With t_i the elution time of an unretained, non-permeating marker that can be obtained from the external porosity (ε_e) as follows:

$$t_i = \frac{L\,\pi r^2 \varepsilon_e}{F} \quad (11)$$

The spatial peak variances (σ^2_x) were plotted against the applied parking time (t_{park}) and the effective diffusion coefficient (D_{eff}) deduced from the slope of this line:

$$\sigma_x^2 = 2 \cdot D_{eff} \cdot t_{park} \quad (12)$$

Bulk diffusion coefficients (D_m) of these molecules in their corresponding mobile phases were measured via the open tubular Taylor-Aris method [34,35]. The test molecules were eluted through a long (L), coiled capillary (D_{coil}) with diameter (d_t) at a low flow rate (L=15.320 m, D_{coil}= 24 cm, d_t= 0,051709 cm, F=0.1 mL/min) under the same mobile phase conditions as for the peak parking experiments [35,36]. D_m was calculated based on the elution time (t) and the variance (σ^2_t) of the analyte:

$$D_m = \frac{d_t^2 \cdot t}{96 \cdot \sigma_t^2} \quad (13)$$

Based on the experimentally determined D_{eff} and D_m values, the reduced b-term coefficient was calculated as follows [37]:

$$b = 2\frac{D_{eff}}{D_m}(1 + k") \quad (14)$$

4. Results

For the in-depth evaluation of pore diffusion, C_{18} reversed-phase columns that were stripped of their stationary phase were used to perform peak parking experiments. Small molecules, that were assumed to be able to access the largest possible fraction of the pore space were used as test molecules and mobile phase conditions were chosen such that no retention would occur for these molecules. Table 3 gives an overview of the test molecules and the corresponding mobile phase conditions that were used for this purpose. To avoid potential ionic interactions between the NO_3^- ion and silanol groups, the ionic marker was prepared in a sufficiently high

concentration (10 mg/mL) [38] and a mobile phase consisting of 20 mM ammonium formate in water, brought to pH= 2.7 with formic acid, was used for the experiments conducted with $NaNO_3$ as test molecule. Table 3 further also shows the values of the external, total and intra-particle (mesoporous zone) porosity obtained for the different combinations of mobile phases and test molecules. The external porosity ε_e was determined in a previous study via inversed size exclusion chromatography (ISEC) experiments and equaled 0.389 [16]. The total porosity ε_T was deduced from the elution time of each test molecule in its respective mobile phase, and corrected for the void time of the system. Slightly larger values of ε_T were obtained when using deuterated acetonitrile and deuterated methanol as test molecules, compared to $NaNO_3$. The values of the intra-particle porosity (ε_{pz}) were subsequently calculated as follows:

$$\varepsilon_{pz} = \frac{\varepsilon_T - \varepsilon_e}{1 - \varepsilon_e} \tag{15}$$

Note that the values of ε_{pz} obtained with deuterated methanol (ε_{pz}= 0.528) and deuterated acetonitrile (ε_{pz}= 0.514) are considerably larger than those obtained with $NaNO_3$ (ε_{pz}= 0.416). This suggests exclusion of the NO_3^- ion from some fraction of the mesopore space, which can either be related to its larger size (see Table 5), preventing it from accessing some parts of the pores, or due to some ionic exclusion. Experiments were therefore also conducted using a higher ionic strength (50 mM ammonium formate instead of 20 mM), but this only slightly increased the ε_T and hence ε_{pz} values (obtained value of ε_{pz}= 0.421), suggesting that NO_3^- is probably unable to sample the mesoporous zone to the same extend as the deuterated compounds. Highly symmetrical peak shapes were moreover obtained for NO_3^-, indicating no (significant) exclusion of the NO_3^- marker due to Donnan exclusion occurred. To further confirm the experimentally obtained values of ε_{pz}, particle porosity values were also calculated based on the following formula [39]:

$$\varepsilon_{pz} = \frac{V_{sp}}{V_{sp} + \frac{1}{\rho_{sk}}} \tag{16}$$

with V_{sp} the specific pore volume (in mL/g) and ρ_{sk} the skeleton density of the particle. According to Neue, the skeleton density of pure, underivatized silica is 2.2 g/mL [39], while the specific pore volume of the underivatized Zorbax Eclipse Plus material used in this study was determined to be 0.43 cm^3/g via BET measurements (information obtained from the manufacturer). Using Eq. (16), this results in a value of ε_{pz}= 0.486, which is close to the values obtained from the elution times of the deuterated molecules, but significantly larger than the

values obtained with $NaNO_3$. This confirms that $NaNO_3$ is probably unable to sample the entire mesoporous volume, while the deuterated molecules are much more suited for this.

Despite the fact that the deuterated molecules resulted in a more realistic assessment of the mesoporous volume of the column, peak parking experiments were subsequently conducted with all three marker molecules for comparison purposes. Performing peak parking experiments in the classical way, i.e., by arresting the flow once the analyte had eluted approximately halfway down the column and resuming the flow after a certain peak parking time (t_{park}) [9,23], the analyte peak was largely influenced by baseline disturbances as shown in Figure 1a. Since the test molecules were unretained under the investigated mobile phase conditions, the analyte peaks eluted very quickly after resuming the flow (t_0=1.3 min at F= 0.2 mL/min). Such short time between switching off and on the flow was insufficient to allow the detector to stabilize, leading to the observed baseline disturbances. Since this made an accurate assessment of the peak parameters via the method of moments difficult, an alternative approach was devised to perform peak parking experiments for unretained compounds. For this purpose, the UHPLC set-up was equipped with two switching valves and two identical columns as shown in Figure 2. In this configuration, the sample was first injected onto stripped column 1 at a flow rate of 0.2 mL/min. When the compound eluted half way down the column, the configuration of the two valves was changed to direct the flow to stripped column 2, blocking off the flow path of stripped column 1. In this way, the mobile phase continued to flow through the detector, while the backpressure was maintained on the system. At the same time, the analyte was parked on stripped column 1 for a specific parking time. After the parking time, the two valves were switched back to open the flow path of stripped column 1, and the analyte was eluted to the detector. A representative chromatogram obtained in this way for $NaNO_3$ is shown in Figure 1b. Comparing this chromatogram with the one obtained in Figure 1a, it is clear that the two-column approach results in a much more stable baseline and a Gaussian peak for the test compound, making moment analysis more straightforward and reliable.

The same set-up was subsequently used to perform peak parking experiments for CD_3OD in pure methanol, CD_3CN in pure acetonitrile and $NaNO_3$ in 20 mM ammonium formate (pH= 2.7) for multiple peak parking time (t_{park} =1, 16, 31, 46, 61, 91 min). The peak variances σ_x^2 obtained for the different parking times were corrected for the system contribution by subtracting the variance obtained for a parking time of 1 min. In this way, any potential band broadening resulting from the switching of the valves was immediately accounted for. The

resulting variances were subsequently plotted as a function of the corrected parking times, obtained by subtracting the same 1min from the experimental parking times and hence leading to corrected t_{park}-values of 15, 30, 45, 60 and 90 min. The obtained curves are shown in Figure 3. From the slopes of these curves, values of D_{eff} were deduced (Table 3). These values were subsequently used to calculate b-term values according to Eq. (14). Note that this equation requires knowledge of the molecular diffusion coefficients (in this study, determined via Taylor-Aris experiments and also shown in Table 3) and the zone retention factor k". In contrast with the more commonly used phase retention factor k', the zone retention factor reflects the time spent in the mesoporous zone (independent of whether this is in the stagnant mobile phase inside the particles, or in the stationary phase) versus the time spent in the moving mobile phase in the interstitial volume (outside the pores). The zone retention factor k" and the phase retention factor k' are related via the following expression [1]:

$$k" = (1 + k')\frac{\varepsilon_T}{\varepsilon_e} - 1 \quad (17)$$

From this equation, it can be deduced that the zone retention factor k'' does not become zero for an unretained compound (k'= 0), but rather turns to $\frac{\varepsilon_T}{\varepsilon_e} - 1$. As such, the zone retention factor reflects that, when residing inside the mesopore space, the unretained compound is still temporarily arrested with respect to the moving mobile phase. Since the values of ε_T obtained for CD_3CN and CD_3OD are slightly larger than that obtained for $NaNO_3$, it is not surprising to see that the latter results in a slightly lower value of k" (k"= 0.65 versus k= 0.81-0.83, see Table 3). These values were subsequently used to calculate the b-term values according to Eq. (14), as shown in Table 3. To extract the values of β_1 from these b-values, it was preferred to use the second-order accurate Eq. (7). It has been demonstrated via numerical studies on random packing geometries with a typical ε_e= 0.384-0.387 [40] that the D_{eff}-values for very small values of k" (as is the case in this study) are much more accurately predicted by Eq. (7) than by the first-order accurate Eq. (6). The value of β_1 can analytically be calculated from Eq. (7) as follows:

$$\beta_1 = \frac{(\varepsilon_e-1)(4+b\varepsilon_e)+\sqrt{(1-\varepsilon_e)^2(4+b\varepsilon_e)^2+8\varepsilon_e\zeta_2(b\varepsilon_e-2)^2}}{4\varepsilon_e\zeta_2(b\varepsilon_e-2)} \quad (18)$$

It has also been demonstrated that for random packings of touching spheres with ε_e= 0.384-0.387, the value of ζ_2= 0.2-0.3. Therefore, values of β_1 were calculated from the experimentally obtained values of b based on Eq. (18) for either ζ_2=0.2 or ζ_2=0.3. The corresponding values of

α_{part} and D_{pz}/D_m were subsequently calculated according to Eqs. (8-9). All obtained values are shown in Table 4 showing that D_{pz}/D_m-values range between 0.57 and 0.63. Since we have for an unretained compound that $K_{A,pz}$= 0, it can be deduced from Eqs. (2-3) that in this case D_{pz}/D_m= γ_{mp}. The values of D_{pz}/D_m shown in Table 4 hence provide a direct experimental measure of mesopore diffusion γ_{mp} and hence also provide an opportunity to model the contributions of the pore hindrance factor F(λ) and the tortuosity τ². For the calculation of F(λ), three frequently used expressions for the calculation of the drag force experienced by a spherical particle when moving near a solid wall, were considered:

$$F(\lambda) = \frac{1-(\frac{9}{8})\lambda ln\lambda^{-1}-1.539\lambda}{1-2\lambda+\lambda^2} \quad (19a)$$

$$F(\lambda) = \frac{1-2.105\lambda+2.0865\lambda^3-1.7068\lambda^5+0.7260\lambda^6}{1-0.75857\lambda^5} \quad (19b)$$

$$F(\lambda) = (1-\lambda^2)(1-2.1044\lambda+2.089\lambda^3-0.948\lambda^5) \quad (19c)$$

In these equations, λ represents the ratio of the molecular size of the analyte to the pore diameter. The molecular sizes of the analytes were determined by calculating the distance between the two most remote atoms in the molecule using Chem3D 16.0 software. The pore size of the bare silica column (before bonding of the stationary phase) was obtained from the manufacturer and was 95 Å. All resulting values for λ and F(λ) are shown in Table 5. For the deuterated molecules, the values of F(λ) are very similar, and amount to 0.88-0.89 using Eq. (19a) and 0.93-0.94 using Eq. (19b-c). For NO_3^-, these values are slightly lower and amount to 0.80 (Eq. 19a) and 0.86 (Eq. 19b-c). The lower values obtained for NO_3^- are entirely in line with the larger molecular size of the latter. The values of F(λ) indicate that, although limited, the pore hindrance of these molecules cannot be neglected despite their small size.

For the calculation of the $\frac{1}{\tau^2}$ -factor in Eq. (4), it has been demonstrated that expressions similar to Eqs. (6-7), based on the effective medium theory, can be used [29]. This is because the space inside the mesopores can also be considered as a tortuous network composed of a binary medium consisting of two phases (the mesopore space and the impermeable silica backbone in this case). It has also been suggested that the intra-particle zone can be represented as the void space in a packing of non-porous nano-spheres [29]. Due to this impermeability, the particle permeability α_{part} in Eq. (8) is strictly zero, leading to a value of β_1= -0.5. When translating this into Eq. (7), the following expression is obtained:

$$\frac{1}{\tau^2} = \frac{1}{\varepsilon_{pz}} \frac{1-(1-\varepsilon_{pz})-\frac{1}{2}\varepsilon_{pz}\zeta_2}{1+\frac{1}{2}(1-\varepsilon_{pz})-\frac{1}{2}\varepsilon_{pz}\zeta_2} \quad (20)$$

Note that in this expression the porosity of the intra-particle zone (ε_{pz}) is used. This value does not reflect the entire meso-pore volume, but only represent the space that is actually accessible to the center of gravity of the probe molecules. Since this is anyhow the volume that is felt by the molecules, this is the right value to use in the models for the diffusion. The parameter ζ_2 again refers to a geometrical three-point parameter, that should have a similar value of 0.2-0.3 if the mesoporous space is considered as a packing of (non-porous) spheres. Table 6 shows the outcome of the multiplication of the different values of $F(\lambda)$ that were obtained using Eqs. (19a-19c) and the values of $1/\tau^2$ calculated with Eq. (20) for ζ_2 varying between 0.2, 0.3 and 0.5. In brackets, the discrepancy with the experimentally obtained value of γ_{mp} is given. Note that the experimental values of γ_{mp} were obtained using values of ζ_2= 0.2 or ζ_2= 0.3 in Eq. (7) for the extraction of β_1 (please refer to Table 4 for the experimental values of γ_{mp}). Focusing on the deuterated molecules, that are assumed to penetrate the mesoporous space to a larger extent than $NaNO_3$, the discrepancy between the experimental and calculated values of γ_{mp} is on average 11.5% (with values ranging between 2% and 21%) when values of ζ_2= 0.2-0.3 are used in Eq. (20), reflecting a mesoporous space that behaves as a packing of non-porous spheres. When the value of ζ_2 in Eq. (20) is increased to 0.5, corresponding to the ζ_2-value for monolithic shaped structures (represented by the tetrahedral skeleton model or TSM) [41], the discrepancy becomes much smaller, and is on average 4% (with values ranging between 0% and 8%). The fact that the experimental γ_{mp} data can be fitted to the second-order Torquato model with a much better agreement when a value of ζ_2=0.5 is used in Eq. (20) is in line with the high ε_{pz}-value (ε_{pz} =0.5). The latter implies that the nano-spheres used in the coacervation process to produce the meso-porous silica particles [32] are not assembled in a conventional random pack configuration (where all spheres are in close contact such that its porosity lies around ε_{pz} =0.4) but rather as a random packing containing a large fraction of (interconnected) holes. This specific geometry (network of large interconnected open spaces running through a solid phase structure) resembles closely that of the simplified TSM, which happens to be characterized by a ζ_2=0.5-value. Additionally, it is observed that the data obtained for deuterated methanol result in a better prediction accuracy when a slightly lower value of $F(\lambda)$ is used (Eq. (19a versus 19b-c)), whereas for deuterated ACN the opposite is true (better prediction accuracy when using Eq. (19b-c versus 19a)). This could indicate that the drag force experienced by deuterated methanol

when moving near the pore wall is slightly larger compared to that of deuterated ACN. This observation could be interpreted in light of the polarity of the methanol molecules and the silanol groups on the pore walls, which would result in a greater affinity for each other.

Finally, to make a comparison with the models proposed by Denoyel et al., the different expressions for F(λ) were divided by the experimentally obtained values of γ_{mp} and fitted to Eq. (5). Again, focusing on the results obtained for the deuterated solvent molecules, this resulted in values of p between p= 0.63 and p=0.93 (Table 6), which is clearly larger than the value of p=0.5 expected for pores resembling an aggregation of non-porous spheres. These p-values therefore confirm our observations that the pore structure of the columns evaluated in this study is more complex than a simple aggregation of spheres.

5. Conclusions

A novel protocol is proposed for the experimental measurement of mesopore diffusion in reversed-phase packed particle columns. For this purpose, peak parking experiments are conducted in columns that have been stripped from their stationary phase using small, deuterated solvent molecules as tracer molecules in mobile phases consisting of the pure solvent. Since no retention occurs under these circumstances, the peaks eluting from the columns after the peak parking experiments are extremely sensitive to baseline disturbances, which leads to a difficult assessment of their first and second moments. Therefore, an instrumental set-up is proposed whereby two identical (in this case stripped) columns are used in parallel, and the flow in one column is arrested by redirecting the flow path from that column to the second column using two switching valves. In this way, the detector used in the set-up is continuously percolated with mobile phase and no baseline disturbances occur when the flow is directed back to the original column after a specific peak parking time. This protocol is used to determine the experimental values of the effective diffusion coefficient for several unretained molecules, and these values are subsequently used to extract the values of the intra-particle coefficient using an expression based on the effective medium theory (EMT). Since no retention occurs for these tracer molecules, the values of intra-particle diffusion immediately lead to an assessment of mesopore diffusion. It is demonstrated that these experimental values can be modeled using typical literature expressions, such as the Brenner and Gaydos, Haberman or Renkin expression, for the calculation of the pore hindrance factor F(λ) and a second-order accurate expression based on the EMT for the calculation of the obstruction factor resulting from the tortuosity of

the pore space ($1/\tau^2$). For the latter, the employed value of the three-point parameter constant ζ_2 is important and, at least for the columns studied in this work, seems to indicate that the geometry of the mesopore space can be represented as a continuous, interconnected series of larger open spaces also encountered in the tetrahedal-skeleton model [41] rather than by the specific, more obstructed through-pore geometry of a conventional random packing of spheres. This is in line with the obtained internal porosity values of ε_{pz}=0.5, where a value of ε_{pz}= 0.4 is rather expected for a conventional random packing of nanospheres. The protocol presented in this study offers a procedure to experimentally determine mesopore diffusion in packed particle columns, which in a next stage can be used to model and understand stationary phase diffusion in similar columns under conditions of retention.

Acknowledgements

Huiying Song is funded by the Research Foundation Flanders (FWO) (post-doctoral grant No. 12Y9818N). Ludovicus Staelens and Johan Nicolai of UCB Pharma (Belgium) are thanked for the kind gift of the triple quadrupole MS. Kris Wolfs is kindly acknowledged for his advice regarding the operation of the LC-MS.

Credit Author Statement

Huiying Song: Conceptualization; Data curation; Formal analysis; Investigation; Methodology; Writing - original draft.

Gert Desmet: Conceptualization; Funding acquisition; Investigation; Methodology; Supervision; Writing - review & editing.

Deirdre Cabooter: Conceptualization; Funding acquisition; Investigation; Methodology; Supervision; Writing - original draft.

References:

[1] G. Desmet, K. Broeckhoven, Equivalence of the different Cm- and Cs- term expressions used in liquid chromatography and a geometrical model uniting them, Anal. Chem. 80 (2008) 8076–8088.

[2] K. Miyabe, G. Guiochon, Surface diffusion in reversed-phase liquid chromatography, J. Chromatogr. A. 1217 (2010) 1713–1734. doi:10.1016/j.chroma.2009.12.054.

[3] H. Song, G. Desmet, D. Cabooter, Assessment of intra-particle diffusion in hydrophilic interaction liquid chromatography and reversed-phase liquid chromatography under

conditions of identical packing structure, J. Chromatogr. A. (2017). doi:10.1016/j.chroma.2017.06.068.

[4] A. Schultze-Jena, M.A. Boon, D.A.M. de Winter, P.J.T. Bussmann, A.E.M. Janssen, A. van der Padt, Predicting intraparticle diffusivity as function of stationary phase characteristics in preparative chromatography, J. Chromatogr. A. 1613 (2020) 460688. doi:10.1016/j.chroma.2019.460688.

[5] C. Giddings, Dynamics of Chromatography: Principles and Theory, New York, 1965.

[6] J. Rybka, A. Höltzel, N. Trebel, U. Tallarek, Stationary-Phase Contributions to Surface Diffusion in Reversed-Phase Liquid Chromatography: Chain Length versus Ligand Density, J. Phys. Chem. C. 123 (2019) 21617–21628. doi:10.1021/acs.jpcc.9b06160.

[7] J. Rybka, A. Höltzel, A. Steinhoff, U. Tallarek, Molecular Dynamics Study of the Relation between Analyte Retention and Surface Diffusion in Reversed-Phase Liquid Chromatography, J. Phys. Chem. C. 123 (2019) 3672–3681. doi:10.1021/acs.jpcc.8b11983.

[8] J. Rybka, A. Höltzel, U. Tallarek, Surface Diffusion of Aromatic Hydrocarbon Analytes in Reversed-Phase Liquid Chromatography, J. Phys. Chem. C. 121 (2017) 17907–17920. doi:10.1021/acs.jpcc.7b04746.

[9] A. Liekens, J. Denayer, G. Desmet, Experimental investigation of the difference in B-term dominated band broadening between fully porous and porous-shell particles for liquid chromatography using the Effective Medium Theory, J. Chromatogr. A. 1218 (2011) 4406–4416. doi:10.1016/j.chroma.2011.05.018.

[10] S.J. Reich, A. Svidrytski, A. Höltzel, W. Wang, C. Kübel, D. Hlushkou, U. Tallarek, Transport under confinement: Hindrance factors for diffusion in core-shell and fully porous particles with different mesopore space morphologies, Microporous Mesoporous Mater. 282 (2019) 188–196. doi:10.1016/j.micromeso.2019.02.036.

[11] S.J. Reich, A. Svidrytski, A. Höltzel, J. Florek, F. Kleitz, W. Wang, C. Kübel, D. Hlushkou, U. Tallarek, Hindered Diffusion in Ordered Mesoporous Silicas: Insights from Pore-Scale Simulations in Physical Reconstructions of SBA-15 and KIT-6 Silica, J. Phys. Chem. C. 122 (2018) 12350–12361. doi:10.1021/acs.jpcc.8b03630.

[12] P. Dechadilok, W.M. Deen, Hindrance factors for diffusion and convection in pores, Ind. Eng. Chem. Res. 45 (2006) 6953–6959. doi:10.1021/ie051387n.

[13] V. Silva, P. Prádanos, L. Palacio, J.I. Calvo, A. Hernández, Relevance of hindrance factors and hydrodynamic pressure gradient in the modelization of the transport of neutral solutes across nanofiltration membranes, Chem. Eng. J. 149 (2009) 78–86.

doi:10.1016/j.cej.2008.10.002.

[14] F. Gritti, I. Leonardis, J. Abia, G. Guiochon, Physical properties and structure of fine core-shell particles used as packing materials for chromatography. Relationships between particle characteristics and column performance, J. Chromatogr. A. 1217 (2010) 3819–3843. doi:10.1016/j.chroma.2010.04.026.

[15] F. Gritti, G. Guiochon, Effect of the surface coverage of C18 -bonded silica particles on the obstructive factor and intraparticle diffusion mechanism, Chem. Eng. Sci. 61 (2006) 7636–7650. doi:10.1016/j.ces.2006.08.070.

[16] H. Song, G. Desmet, D. Cabooter, Evaluation of the Kinetic Performance Differences between Hydrophilic-Interaction Liquid Chromatography and Reversed-Phase Liquid Chromatography under Conditions of Identical Packing Structure, Anal. Chem. 87 (2015) 12331–12339. doi:10.1021/acs.analchem.5b03697.

[17] V. Wernert, R. Bouchet, R. Denoyel, Influence of Molecule Size on Its Transport, Anal. Chem. 82 (2010) 2668–2679.

[18] V. Wernert, R. Bouchet, R. Denoyel, Impact of the solute exclusion on the bed longitudinal diffusion coefficient and particle intra-tortuosity determined by ISEC, J. Chromatogr. A. 1325 (2014) 179–185. doi:10.1016/j.chroma.2013.12.029.

[19] H. Song, G. Desmet, D. Cabooter, Evaluation of the Kinetic Performance Differences between Hydrophilic-Interaction Liquid Chromatography and Reversed-Phase Liquid Chromatography under Conditions of Identical Packing Structure, Anal. Chem. 87 (2015). doi:10.1021/acs.analchem.5b03697.

[20] L. Sun, J.I. Siepmann, M.R. Schure, Monte Carlo Simulations of an Isolated n-Octadecane Chain Solvated in Water - Acetonitrile Mixtures, J. Chem. Theory Comput. 3 (2007) 350–357. doi:10.1021/ct600239z.

[21] J.L. Rafferty, J.I. Siepmann, M.R. Schure, A molecular simulation study of the effects of stationary phase and solute chain length in reversed-phase liquid chromatography, J. Chromatogr. A. 1223 (2012) 24–34. doi:10.1016/j.chroma.2011.11.039.

[22] L.C. Sander, S.A. Wise, C.J. Glinka, Determination of bonded phase thickness in liquid chromatography by small angle neutron scattering, Anal. Chem. 62 (1990) 1099–1101. doi:10.1021/ac00209a025.

[23] H. Song, D. Sadriaj, G. Desmet, D. Cabooter, Methodologies to determine b-term coefficients revisited, J. Chromatogr. A. 1532 (2018). doi:10.1016/j.chroma.2017.11.070.

[24] K. Miyabe, N. Ando, G. Guiochon, Peak parking method for measurement of

molecular diffusivity in liquid phase systems, J. Chromatogr. A. 1216 (2009) 4377–4382. doi:10.1016/j.chroma.2009.02.058.

[25] F. Gritti, G. Guiochon, Multi-location peak parking method: An important new tool for the study of mass transfer kinetics in liquid chromatography, J. Chromatogr. A. 1218 (2011) 896–906. doi:10.1016/j.chroma.2010.12.024.

[26] F. Gritti, G. Guiochon, Importance of Sample Intraparticle Diffusivity in Investigations of the Mass Transfer Mechanism in Liquid Chromatography, AIChE J. 57 (2011) 346–358.

[27] F. Gritti, G. Guiochon, New Insights on Mass Transfer Kinetics in Chromatography, AIChE J. 57 (2011) 333–345.

[28] K. Broeckhoven, D. Cabooter, F. Lynen, P. Sandra, G. Desmet, Errors involved in the existing B-term expressions for the longitudinal diffusion in fully porous chromatographic media. Part II: Experimental data in packed columns and surface diffusion measurements, J. Chromatogr. A. 1188 (2008). doi:10.1016/j.chroma.2008.02.058.

[29] G. Desmet, S. Deridder, Effective medium theory expressions for the effective diffusion in chromatographic beds filled with porous, non-porous and porous-shell particles and cylinders. Part I: Theory, J. Chromatogr. A. 1218 (2011) 32–45. doi:10.1016/j.chroma.2010.10.087.

[30] D. Cabooter, F. Lynen, P. Sandra, G. Desmet, Total pore blocking as an alternative method for the on-column determination of the external porosity of packed and monolithic reversed-phase columns, J. Chromatogr. A. 1157 (2007) 131–141.

[31] D. Cabooter, J. Billen, H. Terryn, F. Lynen, P. Sandra, G. Desmet, Detailed characterisation of the flow resistance of commercial sub-2 ??m reversed-phase columns, J. Chromatogr. A. 1178 (2008) 108–117.

[32] R. Iler, H. McQueston, US Patent 4010242 Uniform oxide microspheres and a process for their manufacture, 1977.

[33] Y. Vanderheyden, K. Broeckhoven, G. Desmet, Comparison and optimization of different peak integration methods to determine the variance of unretained and extra-column peaks, J. Chromatogr. A. 1364 (2014) 140–150. doi:10.1016/j.chroma.2014.08.066.

[34] G. Taylor, Dispersion of Soluble Matter in Solvent Flowing Slowly through a Tube, Proc. R. Soc. Lond. A. 219 (1953) 186–203. doi:10.1098/rspa.1953.0139.

[35] H. Song, Y. Vanderheyden, E. Adams, G. Desmet, D. Cabooter, Extensive database of

liquid phase diffusion coefficients of some frequently used test molecules in reversed-phase liquid chromatography and hydrophilic interaction liquid chromatography, J. Chromatogr. A. 1455 (2016) 102–112. doi:10.1016/j.chroma.2016.05.054.

[36] J. Li, P.W. Carr, Accuracy of empirical correlations for estimating diffusion coefficients in aqueous organic mixtures., Anal. Chem. 69 (1997) 2530–2536. doi:doi: 10.1021/ac961005a.

[37] J.H. Knox, H.P. Scott, B and C terms in the Van Deemter equation for liquid chromatography, J. Chromatogr. A. 282 (1983) 297–313. doi:doi: DOI: 10.1016/S0021-9673(00)91609-1.

[38] F.Z. Oumada, M. Rosés, E. Bosch, Inorganic salts as hold-up time markers in C18 columns, Talanta. 53 (2000) 667–677. doi:10.1016/S0039-9140(00)00556-7.

[39] U.D. Neue, HPLC Columns: Theory, Technology and Practice, Wiley-VCH, New York, 1997.

[40] S. Deridder, G. Desmet, Calculation of the geometrical three-point parameter constant appearing in the second order accurate effective medium theory expression for the B-term diffusion coefficient in fully porous and porous-shell random sphere packings, J. Chromatogr. A. 1223 (2012) 35–40. doi:10.1016/j.chroma.2011.12.004.

Figure captions

Figure 1: Representative peak parking chromatograms obtained for $NaNO_3$ (10 mg/mL), obtained using (a) the classical peak parking method; (b) the adapted peak parking method with two switching valves to couple two identical columns in parallel to the UHPLC. Mobile phase is 20 mM ammonium acetate pH 2.7. Peak parking time was 60 min.

Figure 2: The adapted experimental set-up for peak parking experiments wherein two switching valves are used to couple two identical columns in parallel to the UHPLC. To maintain a constant backpressure, identical connection tubing was used between the left valve and the inlets of columns 1 and 2 (I.D x L: 100 µm x 150 mm, green), and the outlets of columns 1 and 2 and the right valve (I.D x L: 75 µm x 250 mm, purple).

Figure 3: Plots of σ_x^2 versus parking time (t_{park}) for **(a)** CD_3CN in ACN, **(b)** CD_3OD in MeOH and **(c)** $NaNO_3$ in 20 mM ammonium acetate pH 2.7, obtained using the experimental set-up shown in Figure 2. Error bars indicate the standard deviations obtained by performing each peak parking experiment four times consecutively. All data were analyzed via moments analysis. The regression equations and R^2 values are also shown.

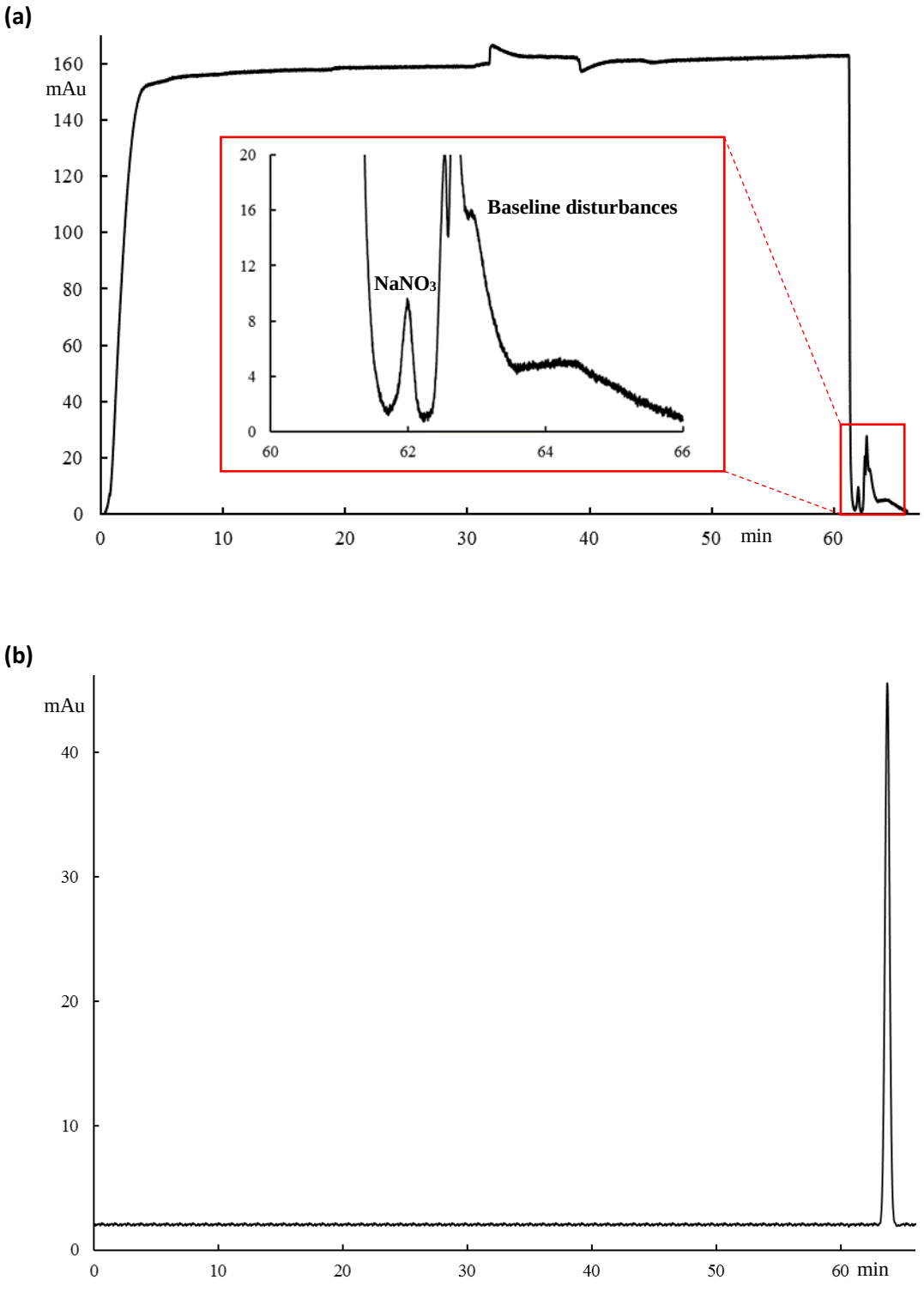
(a)
160
mAu
140
120
100
80
60
40
20
0
0
10
20
30
40
50
min
60
20
16
12
8
4
0
60
62
64
66
NaNO3
Baseline disturbances
(b)
mAu
40
30
20
10
0
0
10
20
30
40
50
60
min

Figure 1

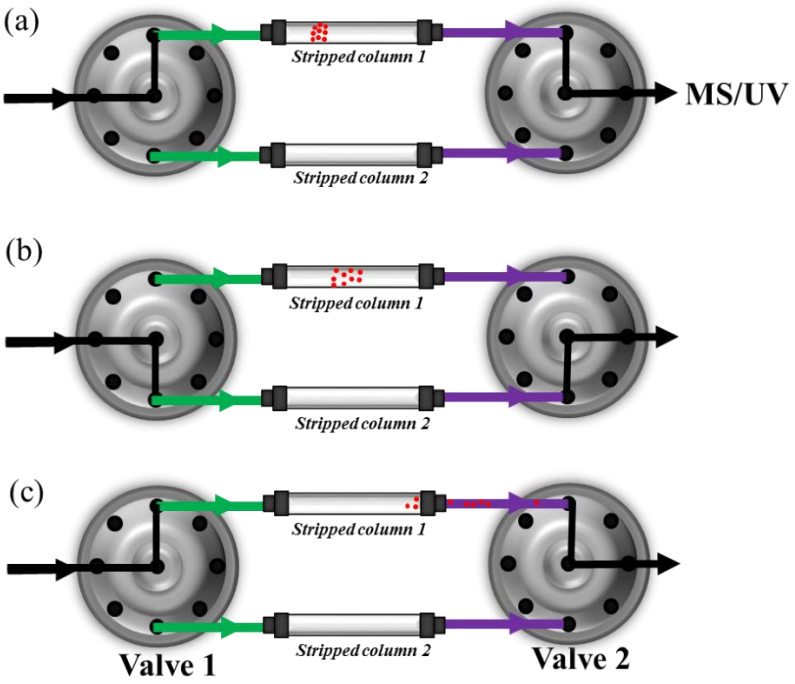
(a)
Stripped column 1
MS/UV
Stripped column 2
(b)
Stripped column 1
Stripped column 2
(c)
Stripped column 1
Stripped column 2
Valve 1
Valve 2

Figure 2

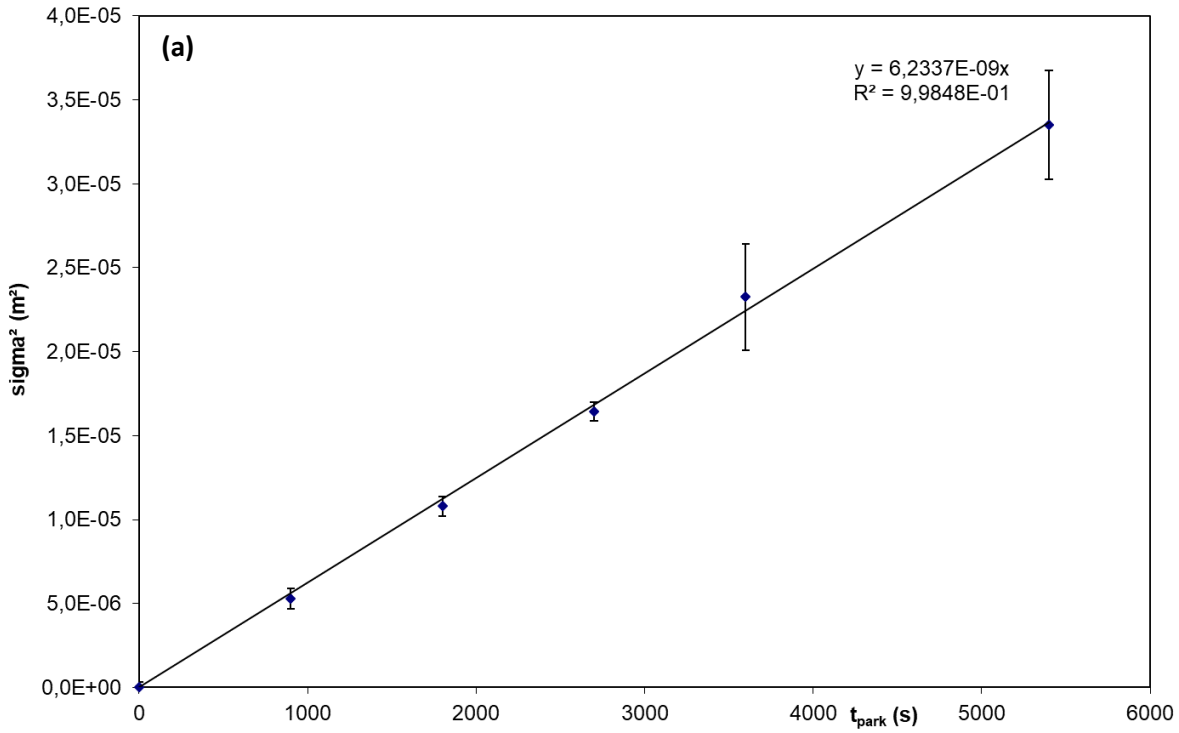
(a)
y = 6,2337E-09x
R² = 9,9848E-01
sigma² (m²)
4,0E-05
3,5E-05
3,0E-05
2,5E-05
2,0E-05
1,5E-05
1,0E-05
5,0E-06
0,0E+00
0
1000
2000
3000
4000
5000
6000
t_park (s)

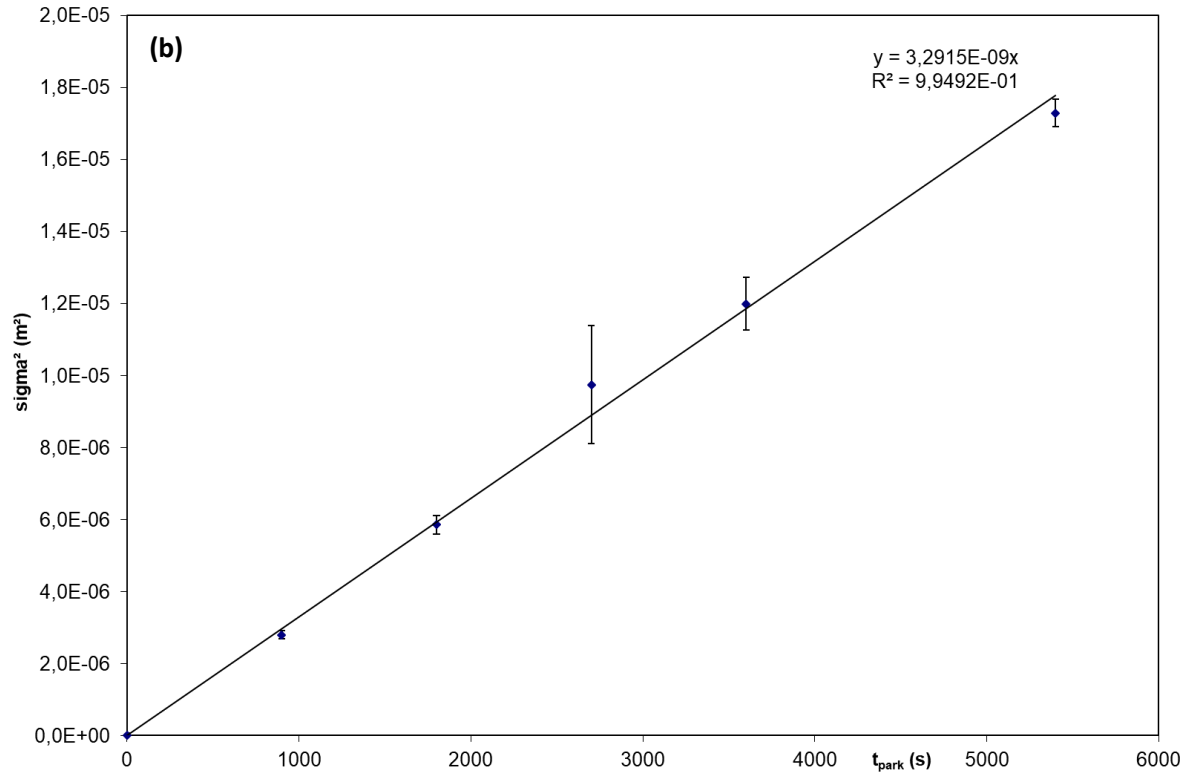
(b)
y = 3,2915E-09x
R² = 9,9492E-01
sigma² (m²)
2,0E-05
1,8E-05
1,6E-05
1,4E-05
1,2E-05
1,0E-05
8,0E-06
6,0E-06
4,0E-06
2,0E-06
0,0E+00
0
1000
2000
3000
4000
5000
6000
t_park (s)

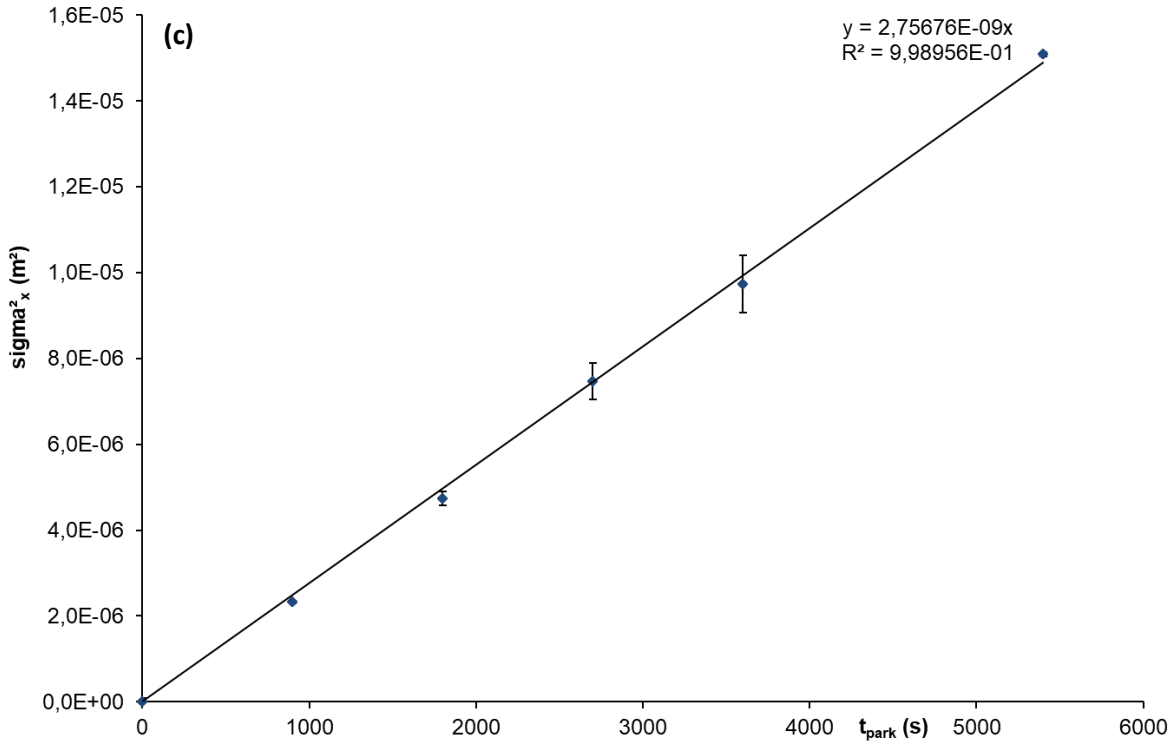
(c)
y = 2,75676E-09x
R² = 9,98956E-01
1,6E-05
1,4E-05
1,2E-05
1,0E-05
8,0E-06
6,0E-06
4,0E-06
2,0E-06
0,0E+00
sigma² x (m²)
0
1000
2000
3000
4000
5000
6000
t park (s)

Figure 3

Table 1: Specific parameters of the Zorbax Eclipse Plus C18 material

Pore size (Å) (bare silica material)	95
Particle size (µm)	5
Surface area (m^2/g)	165
Carbon load (%)	9%
Pore volume (cm^3/g)	0.43

Table 2: MS optimized parameters for CD_3OD and CD_3CN. The declustering potential (DP), focusing potential (FP), entrance potential (EP), nebulization gas pressure (NEB), curtain gas pressure (CUR), source temperature (TEM) and ionspray voltage (IS) are shown.

	Mass (Da)	DP (V)	FP (V)	EP (V)	NEB (psi)	CUR (psi)	IS (V)	TEM (°C)	Heater gas (L/min)
CD_3OD	36.034	140	150	5	10	8	5500	550	7
CD_3CN	45.022	55	165	14	14	11	5500	550	7

Table 3: Test molecules and corresponding mobile phase conditions used for the assessment of the total porosity ε_T and the internal porosity ε_{pz}. The interstitial porosity ε_e was determined via ISEC experiments in [12]. Effective and molecular diffusion coefficients were determined as described in the text. The b-term value was calculated according to Eq. (14).

Test molecule	CD_3CN	CD_3OD	$NaNO_3$
Mobile phase	ACN	MeOH	20 mM ammonium formate (pH= 2.7)
ε_e	0.389	0.389	0.389
ε_T	0.703	0.712	0.644
ε_{pz}	0.514	0.528	0.416
k”	0.81	0.83	0.65
D_{eff}	3.12×10^{-9}	1.65×10^{-9}	3.12×10^{-9}
D_m	4.13×10^{-9}	2.20×10^{-9}	4.13×10^{-9}
D_{eff}/D_m	0.7554	0.7475	0.7431
b	2.73	2.73	2.46

Table 4: Calculated values of β_1 according to Eq. (18) with ζ_2= 0.2 or ζ_2= 0.3. Values of ε_e and b can be found in Table 3. The obtained values of β_1 were consequently used to calculate α_{part} and D_{pz}/D_m according to Eqs. (8-9). The thus obtained values of D_{pz}/D_m reflect the experimentally measured values of γ_{mp}.

	Test molecule	CD_3CN	CD_3OD	$NaNO_3$
ζ_2	Mobile phase	ACN	MeOH	20 mM ammonium formate (pH= 2.7)
0.2	β_1	-0.29	-0.30	-0.34
	α_{part}	0.32	0.31	0.24
	D_{pz}/D_m	0.6191	0.5879	0.5792
0.3	β_1	-0.29	-0.30	-0.34
	α_{part}	0.32	0.31	0.25
	D_{pz}/D_m	0.6259	0.5947	0.5910

Table 5: Molecular sizes of the test molecules considered for the peak parking experiments, obtained via Chem3D 16.0 software. Values of F(λ) calculated via Eqs. (19a-c).

Test molecule	CD_3CN	CD_3OD	$NaNO_3$
Mobile phase	ACN	MeOH	20 mM ammonium formate (pH= 2.7)
Molecular size (Å)	3.19	2.87	6.25
λ	0.034	0.030	0.066
F(λ) Eq (17a)	0.88	0.89	0.80
F(λ) Eq (17b)	0.93	0.94	0.86
F(λ) Eq (17c)	0.93	0.94	0.86
F(λ) Eq (17d)	0.82	0.83	0.70

Table 6: Calculated values of γ_{mp}, obtained by multiplying the different values of $F(\lambda)$ obtained via Eqs. (19a-d) with the values of $1/\tau^2$, calculated via Eq. (20) wherein the value of ζ_2 has been varied between 0.2 and 0.3, to approximate the silica backbone as a packing of non-porous particles, and a value of 0.5, to approximate the silica backbone as a continuous monolith-like network. The values between brackets indicate the discrepancy between the experimentally obtained values of γ_{mp}, using either a value of ζ_2=0.2 in Eq. (7) or a value of ζ_2=0.3 in Eq. (7) (in bold) for the extraction of β_1. Discrepancies were calculated as the absolute difference between the experimental and calculated value, divided by the experimental value × 100%. The last row shows the p-values obtained by fitting $F(\lambda)/\gamma_{mp}$ to Eq. (5) (γ_{mp}: experimentally obtained).

Test molecule	CD_3CN		CD_3OD		$NaNO_3$	
ζ_2 in Eq. (18)	$F(\lambda)$=0.88	$F(\lambda)$=0.93	$F(\lambda)$=0.89	$F(\lambda)$=0.94	$F(\lambda)$=0.80	$F(\lambda)$=0.86
ζ_2=0.2	0.663 (7%) **(6%)**	0.701 (13%) **(12%)**	0.675 (15%) **(13%)**	0.712 (21%) **(20%)**	0.575 (1%) **(3%)**	0.618 (7%) **(5%)**
ζ_2=0.3	0.640 (3%) **(2%)**	0.677 (9%) **(8%)**	0.652 (11%) **(10%)**	0.687 (17%) **(16%)**	0.552 (5%) **(7%)**	0.593 (2%) **(0%)**
ζ_2=0.5	0.591 (5%) **(6%)**	0.625 (1%) **(0%)**	0.603 (3%) **(1%)**	0.636 (8%) **(7%)**	0.504 (13%) **(15%)**	0.542 (6%) **(8%)**
p [17,18]	0.63 **0.63**	0.75 **0.73**	0.80 **0.77**	0.93 **0.90**	0.43 **0.40**	0.56 **0.52**